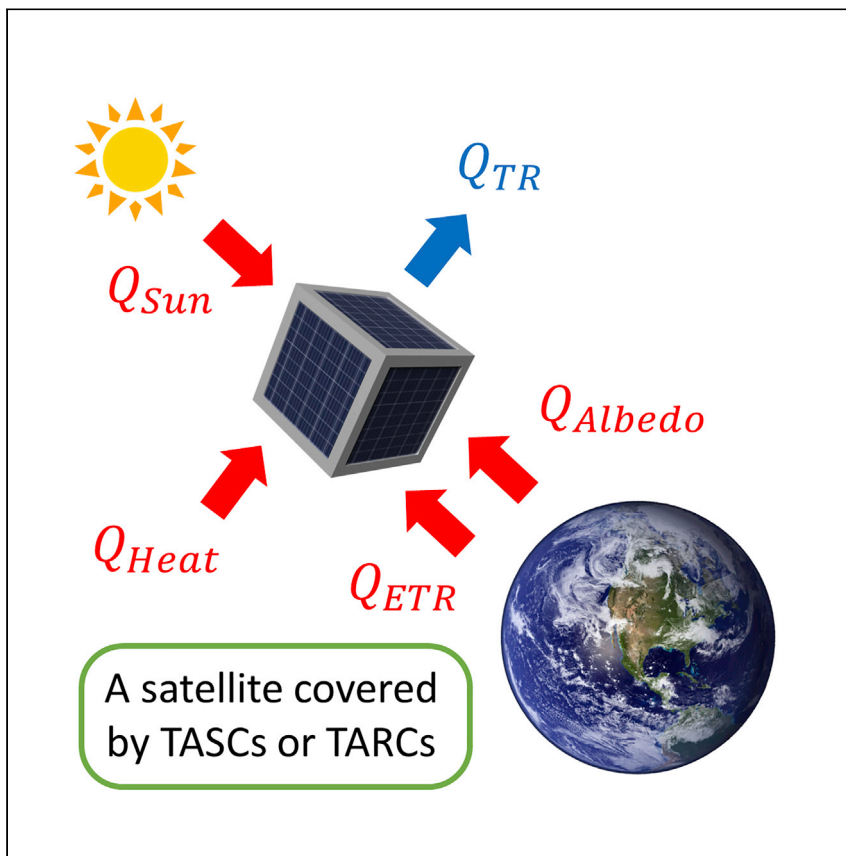


Report

Reducing temperature swing of space objects with temperature-adaptive solar or radiative coating



Kaichen Dong, Derick Tseng,
Jiachen Li, Sorren Warkander,
Jie Yao, Junqiao Wu

wuj@berkeley.edu

Highlights

TASCs and TARCs are promising for passive temperature management in outer space

TASCs and TARCs do not bring in extra mass, volume, or power burdens to spacecrafts

The thermal performance of TASCs and TARCs is simulated with satellite thermal models

Simulations show a temperature swing as low as 5.3°C in a 1U-CubeSat covered by TARCs

Advanced high-performance passive temperature management technologies without additional mass/volume/power burdens are required for space exploration. Dong et al. propose use of emerging temperature-adaptive solar or radiative coatings (TASCs or TARCs, respectively) on space objects and simulate their temperature-regulation performance with satellite thermal models, demonstrating the potential of TARCs and TARCs in outer space.

Dong et al., Cell Reports Physical Science 3, 101066
October 19, 2022 © 2022 The Author(s).
<https://doi.org/10.1016/j.xcrp.2022.101066>



Report

Reducing temperature swing of space objects with temperature-adaptive solar or radiative coating

Kaichen Dong,^{1,2} Derick Tseng,¹ Jiachen Li,^{1,2} Sorren Warkander,^{1,2} Jie Yao,^{1,2} and Junqiao Wu^{1,2,3,*}

SUMMARY

Lacking the atmosphere for temperature neutralization, objects in outer space without thermal control undergo large temperature swings. Effective temperature management technologies (TMTs) are essential to avoid undesirable effects caused by extreme thermal conditions. However, existing high-performance TMTs impose additional burden on the limited mass and power budgets of space-crafts. Very recently, temperature-adaptive solar coatings (TASCs) and temperature-adaptive radiative coatings (TARCs) emerged as novel light-weight, energy-free temperature-regulation approaches for terrestrial objects with excellent thermal performance. Here, we simulate and present the great potential of TASCs and TARCs as future passive TMTs for space objects. A case study of a geosynchronous satellite with body-mounted solar panels covered by TARC exhibits an interior temperature swing as small as 20.3°C–25.6°C in an orbital period even with solar eclipses. These findings provide insight into the superior performance of TASCs and TARCs in space and will promote their application in extraterrestrial missions.

INTRODUCTION

Temperature maintenance and regulation are vital to space-crafts and astronauts due to the extremely hostile environments in space.^{1,2} The temperature of a space object can easily change by many hundreds of degrees (−220°C to +220°C) depending primarily on solar irradiance received by and heat radiated from the object,² imposing fatal threats to all components and crew (for manned space missions).^{3,4} Moreover, such high temperature swings also introduce instrumental misalignment,⁵ large noise signals,^{6,7} and thermal cycling damages to mechanical structures.⁸ To ensure normal operation of components and survival of crew, massive temperature swings must be avoided by advanced thermal management technologies (TMTs).^{9,10}

Existing TMTs that have already been applied to space objects (including space-crafts and spacesuits) are categorized as active and passive strategies according to their need for power input. Active TMTs—including electrical heaters,¹¹ cryo-coolers,¹² thermoelectric coolers,¹³ and fluid loops¹⁴—consume electricity to provide accurate temperature control of space objects. However, they typically require extra mass, volume, and power, so they are generally only used with high heat loads in large space-crafts.¹⁰ On the contrary, passive TMTs offer power-free control of temperatures and are thus favorable in power-sensitive and small space objects. However, conventional passive TMTs—such as paints and coatings,¹⁵ multi-layer insulation materials,¹⁶ and sun shields¹⁷—are limited by their static radiative heat transfer properties and are thus incapable of reducing both the high and low

¹Department of Materials Science and Engineering, University of California, Berkeley, Berkeley, CA 94720, USA

²Materials Sciences Division, Lawrence Berkeley National Laboratory, Berkeley, CA 94720, USA

³Lead contact

*Correspondence: wuj@berkeley.edu

<https://doi.org/10.1016/j.xcpr.2022.101066>



temperature extremes in thermal cycles. Some advanced passive TMTs—like passive thermal louvers,¹⁸ deployable radiators,¹⁹ thermal switches,²⁰ and phase-change thermal storage units²¹—have been employed for temperature-adaptive thermal control, but unfortunately, they come at the cost of high extra mass and volume. It is therefore essential to develop a high-performance passive TMT without additional mass and volume requirements.

Very recently, temperature-adaptive radiative coatings (TARCs) were invented,^{22–28} which “intelligently” and automatically adjust their thermal radiation according to surface temperatures. At high temperatures, they strongly emit thermal radiation to dissipate heat into outer space; at lower temperatures, they automatically turn off radiation to retain heat. The solar absorptivity of TARCs is temperature independent. Neither power input nor manual intervention are required during this process. Though first invented for terrestrial objects like house roofs, this emerging technology shows great potential in space applications. Such thin, flexible, lightweight, and power-free coatings are expected to dramatically reduce the temperature swings experienced by space objects.^{22,25,26}

In this work, we systematically simulated the temperature-regulation performance of temperature-adaptive coatings in space missions with three different models: (1) a two-dimensional (2D) flat surface, (2) a 3D cube (regular hexahedron), and (3) a geosynchronous 1U-CubeSat²⁹ orbiting Earth. In those models, temperature-adaptive solar coatings (TASCs) and TARCs were compared. TASCs work in a similar way as TARCs except that their solar absorptivity, as opposed to thermal emissivity, is switched in response to temperature change, while their thermal emissivity stays a constant. Both TASCs and TARCs significantly cut down the temperature swing compared with the original surface of the space object that is not temperature adaptive. Because the only thermal interaction with the environment in space is electromagnetic radiation, we found that although the relative advantages between TASCs and TARCs vary from mission to mission, TARCs evidently outperform TASCs for Earth satellites in orbits with solar eclipses. Furthermore, we simulated the scenarios where TASCs and TARCs hypothetically have 100% transmission in the wavelength range of 0.4–1.1 μm so that they can cover the solar panels (SPs) of spacecrafts without influencing the SP performance.^{30,31} We revealed that the performance in limiting the temperature swing deteriorates for TASCs but remains nearly the same for TARCs. The above analyses were followed by a case study where a geosynchronous CubeSat is covered by an experimentally demonstrated TARC (hereafter called a “real-TARC”) with published data.²² In-depth, transient thermal analysis of body-mounted SPs and interior satellite components were conducted, showing the extraordinary performance of TARCs in reducing temperature swings. As such, TARCs show great promise as a new passive TMT in space missions and offer new temperature-regulation solutions for a diverse range of space objects such as space stations, satellites, spacesuits, and even extraterrestrial bases.³²

RESULTS AND DISCUSSION

Temperature swings of space objects

The extraterrestrial (AM0) solar spectrum³³ and a typical black-body radiation spectrum are shown in Figure 1A. Unlike the terrestrial thermal emitters that are limited in and optimized for the 8–13 μm atmospheric transparency window,³⁴ the thermal emitters in space are not spectrally limited due to the vacuum environment. As a result, the energy flux of thermal radiation is enhanced for objects in space to a level

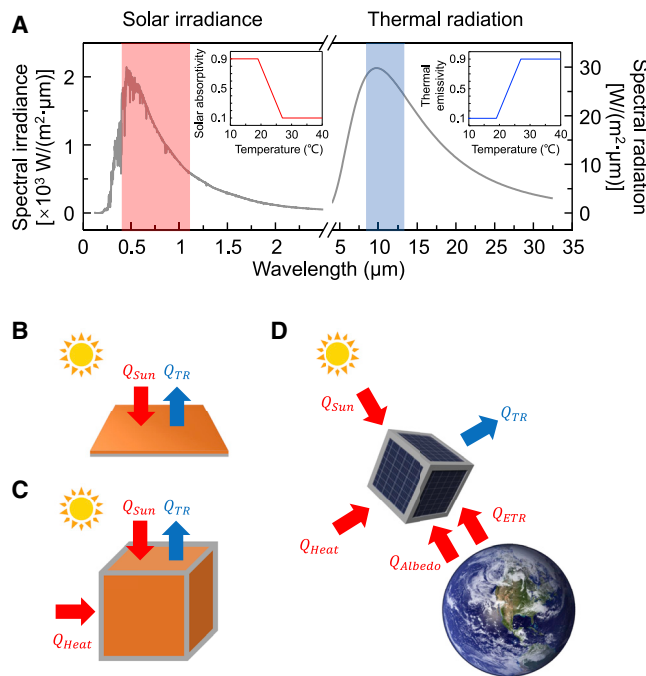


Figure 1. Theoretical schemes

(A) Spectra of AM0 solar irradiance (left) and black-body radiation at 23°C calculated by Planck's law (right). The red and blue boxes indicate the ideal 100% transmission band for TASCs or TARC_s covering solar panels and the atmospheric transmission window for terrestrial thermal emitters, respectively. Inset: temperature-adaptive solar absorptivity of TASCs (left) and temperature-adaptive thermal emissivity of TARC_s (right) analyzed in this work.

(B–D) Schematic diagrams of the 2D board model (B), the 3D cube model (C), and the CubeSat model (D). Q_{Sun} , Q_{TR} , Q_{Heat} , Q_{Albedo} , and Q_{ETR} are heat transfer power from solar irradiance (heating), thermal radiation of the CubeSat (cooling), interior satellite components (heating), Earth albedo (heating), and thermal radiation of Earth (heating), respectively.

that could outweigh the solar heating, which necessitates the comparison between TASCs and TARC_s in their temperature-regulation performance in outer space.

Hence, we compared temperature swings of space objects using eight different TASCs and TARC_s whose solar absorptivity (α) and thermal emissivity (ϵ) are defined as follows (see Table S3 for details):

- (1) TASCs with a switchable α and a low ϵ (0.1) or a high ϵ (0.9).
- (2) SP-compatible TASCs with a switchable α and a low ϵ (0.1) or a high ϵ (0.9).
- (3) TARC_s with a switchable ϵ and a low α (0.1) or a high α (0.9).
- (4) SP-compatible TARC_s with a switchable ϵ and a low α (0.1) or a high α (0.9).

The switchable α of TASCs and switchable ϵ of TARC_s are shown in the left and right insets of Figure 1A, respectively. The 19°C–27°C temperature range for the switching transition is taken from previous work,²² and the target temperature for stabilization is $T_{set} = 23^\circ\text{C}$ in the middle of the switching range (Note S1; Table S1). Since spacecrafts, especially miniature satellites, are power-efficient systems equipped with large-area body-mounted SPs,³⁵ the compatibility with SPs will significantly expand the total applicable area of TASCs or TARC_s on spacecrafts. In our simulation, SP-compatible TASCs and TARC_s are those that have everything else the same as the normal TASCs and TARC_s but with 100% transmittance over the primary spectral response range (0.4–1.1 μm) of photovoltaics (PVs)^{30,31} so that they can be applied on top of SPs

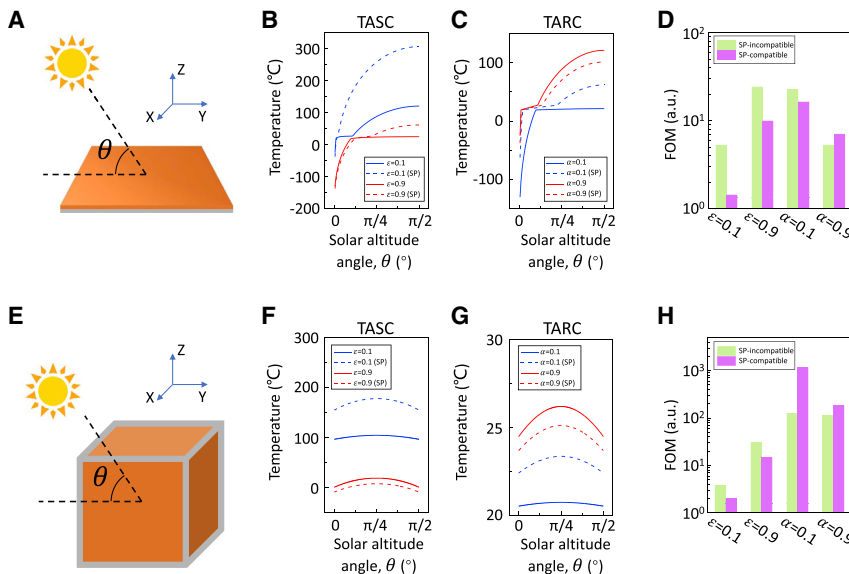


Figure 2. Fundamental thermal analysis models for TASCs and TARCs

(A) A schematic diagram of the 2D board model.

(B and C) Static surface temperatures as functions of θ for boards covered by TASCs (B) or TARC (C), where SP represents SP compatible.

(D) Extracted FOMs for the cases in (B) and (C).

(E) A schematic diagram of the 3D cube model.

(F and G) Static surface temperatures as functions of θ for cubes covered by TASCs (F) or TARC (G), where SP represents SP compatible.

(H) Extracted FOMs for the cases in (F) and (G).

([Note S2](#); [Figure S1](#)). Note that in this simulation, the SPs beneath SP-compatible TASCs or TARC are assigned with a PV efficiency of 25% and a reflectance of 10%,^{36,37} leading to 65% of the solar energy in 0.4–1.1 μm converted into heat in SPs for SP-compatible cases. Apart from that 0.4–1.1 μm range in the SP-compatible scenario, all TASCs and TARC have 0% transmittance in both solar and thermal spectra. The above coatings were analyzed using three different models ([Figures 1B–1D](#)).

We first calculated the surface temperature of a 2D board in space under solar irradiance ([Figure 1B](#)), with the top surface covered by TASC or TARC and the bottom surface completely insulated from the environment. Such a 2D board can be considered as a basic component of various 3D objects, thus providing valuable information on the behavior of more complex objects. A thermal equilibrium state is achieved when the Q_{Sun} equals Q_{TR} at the top surface:

$$\begin{cases} Q_{\text{Sun}}(\theta, T) = Q_{\text{TR}}(T) \\ Q_{\text{Sun}}(\theta, T) = H_{\text{Sun}} \times \sin \theta \times \alpha(T) \times A \\ Q_{\text{TR}}(T) = (H_{\text{SB}}(T) - H_{\text{SB}}(T_{\text{space}})) \times \varepsilon(T) \times A \end{cases}, \quad (\text{Equation 1})$$

where $H_{\text{Sun}} = 1,367 \text{ W/m}^2$ is the solar energy heat flux for Earth satellites³⁸ and $H_{\text{SB}}(T)$ is the black-body radiation flux by the Stefan-Boltzmann's law.^{38–40} With a background space temperature of $T_{\text{space}} = 2.7 \text{ K}$,^{39,40} the static surface temperature T as a function of solar altitude angle θ ([Figure 2A](#)) is calculated for all TASCs and TARC, and the results are compared in [Figures 2B](#) and [2C](#) (see [Note S3](#) and [Figures S2](#) and [S3](#) for more details). Note that all temperatures at $\theta = 0^\circ$ are 2.7 K and thus are excluded from the plots for clarity. Most spacecraft components achieve optimal performance near room temperatures ([Note S1](#)), so we define the dimensionless figure of merit (FOM) for temperature management as

$$FOM = \frac{T_{set} \times \int_0^{\pi/2} d\theta}{\int_0^{\pi/2} |T(\theta) - T_{set}| d\theta}. \quad (\text{Equation 2})$$

Obviously, the FOM describes the relative extent of T deviating from T_{set} integrated over an entire period. A high value of FOM is desired, as it indicates a small temperature swing in the space mission. The FOM would be equal to infinity if the temperature swing is ideally zero (T is constant and $= T_{set}$), close to 1 if the temperature is constant and near 0 K, and approaching zero if the temperature experiences a very large swing ($|T(\theta) - T_{set}| \gg 0$).

Due to the broadband thermal emission in space, the temperature swings for the cases of TASCs and TARC斯 are similar in [Figures 2B](#) and [2C](#). This differs substantially from terrestrial scenarios where solar heating power dominates over thermal radiation because the latter is limited to a narrow sky window.³⁴ Another conclusion is the static ϵ (α) should be optimized to achieve smaller temperature swings for TASCs (TARC斯): one order-of-magnitude change in FOM can be found between optimized and unoptimized TASCs and TARC斯 ([Figure S3](#)). Moreover, when temperature-adaptive coatings are made SP compatible to cover SPs, the temperature-management performance of TASCs worsens due to the non-temperature-adaptive α in the 0.4–1.1 μm band. The FOM of TASC ($\epsilon = 0.1$ or 0.9) is decreased by a factor of 3.7 or 2.4 when SP compatibility is enforced.

To better identify the temperature swing of actual 3D objects, we then simulated a cube whose six surfaces are all covered by identical TASCs or TARC斯 ([Figure 1C](#)). The static temperature for such a cube is calculated by

$$\begin{cases} Q_{Sun}(\theta, T) + Q_{Heat} = Q_{TR}(T) \\ Q_{Sun}(\theta, T) = H_{Sun} \times (\sin \theta + \cos \theta) \times \alpha(T) \times A \\ Q_{TR}(T) = (H_{SB}(T) - H_{SB}(T_{space})) \times \epsilon(T) \times A \times 6 \end{cases}. \quad (\text{Equation 3})$$

Based on the typical design of a 1U-CubeSat, the area of each surface (A) is set at 0.01 m^2 .²⁹ Here, the CubeSat is assumed to be in the “working” mode with high power consumption throughout the simulated period, and the interior heating power (Q_{Heat}) is set at a constant 5 W.^{41,42} In our calculation, for simplicity, the sunbeam direction is in the yz plane ([Figure 2E](#)), i.e., it is normal to the $-y$ and $+z$ cube surfaces when $\theta = 0^\circ$ and $\pi/2$, respectively.

Though [Figures 2F](#) and [2G](#) verify that both TASCs and TARC斯 help reduce the temperature swings, TARC斯 excel in maintaining a smaller temperature swing because the total physical area of thermal emission (all six surfaces) greatly exceeds that of solar absorption (three surfaces at most), regardless of SP compatibility ([Figure 2H](#)). The FOM of SP-compatible TASC ($\epsilon = 0.1$) is surprisingly 99.8% lower than that of the SP-compatible TARC ($\alpha = 0.1$). Calculation details and results with other sunbeam directions can be found in [Note S4](#) and [Figures S4](#) and [S5](#).

Additionally, we conducted a more comprehensive thermal analysis by calculating the transient temperature of a geostationary 1U-CubeSat when the Earth is at the December solstice ([Figure 3A](#)). In such an orbit, the CubeSat does not experience solar eclipses. Note that in this model we do not consider the inhomogeneous temperature distribution inside the CubeSat. The orbital period of the CubeSat is $\sim 1,436$ min, and the revolution of the Earth is not considered. The calculation starts at $t = -24$ h, and the CubeSat is at position p_0 with a temperature of 0°C.

The transient temperature is calculated by (see [Note S5](#) and [Table S4](#) for details)

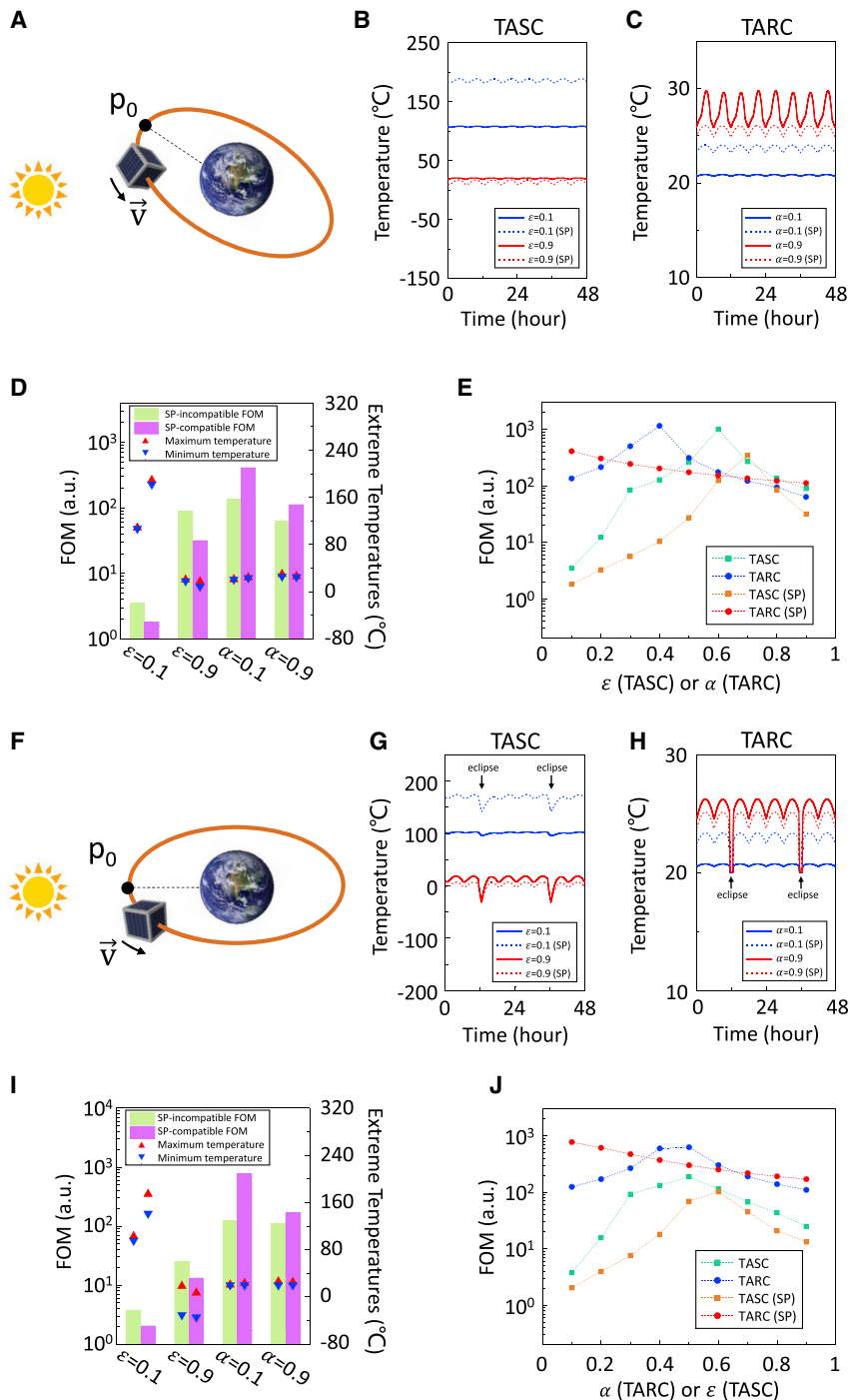


Figure 3. Transient thermal analysis of a 1U-CubeSat covered by TASCs or TARCs

(A) A schematic diagram of the geostationary CubeSat model when the Earth is at the December solstice.

(B) and (C) Transient temperatures of the CubeSat covered by TASCs or TARCs.

(D) Extracted FOMs and extreme temperatures for the cases in (B) and (C).

(E) FOMs as functions of static ε (or α) for TASCs (or TARCs) for the orbit in (A).

(F) A schematic diagram of the geosynchronous CubeSat model in the ecliptic plane.

(G) and (H) Transient temperatures of the CubeSat covered by TASCs or TARCs.

(I) Extracted FOMs and extreme temperatures for the cases in (G) and (H).

(J) FOMs as functions of static ε (or α) for TASCs or TARCs for the orbit in (F).

$$Q_{Sun}(T, t) + Q_{Heat} + Q_{Albedo}(T, t) + Q_{ETR}(T, t) - Q_{TR}(T, t) = m \times c \times \frac{dT}{dt}. \quad (\text{Equation 4})$$

As shown in [Figure 1D](#), apart from direct solar heating and thermal radiative cooling, the temperature of Earth-orbiting satellites also depends on the heating from the sunlight reflected by the Earth (known as albedo) as well as thermal infrared (IR) radiation emitted from Earth, both of which can be regulated by temperature-adaptive coatings.

The transient temperatures of the CubeSats covered by different TASCs or TARCs are depicted in [Figures 3B](#) and [3C](#), respectively. The results show that the performance of TARCs in regulating the temperature around T_{set} is less sensitive to the value of the static α , while an unoptimized static ϵ can severely increase the temperature swing of a CubeSat covered by TASCs. Here, a static α or ϵ means the α or ϵ does not change with temperature. Furthermore, the SP compatibility deteriorates the temperature-regulation performance of TASCs due to the uncontrolled solar absorptivity in 0.4–1.1 μm , while SP-compatible TARCs behave well even with SP compatibility. The FOMs and extreme temperatures in [Figure 3D](#) also verify the above conclusions. Note that the FOM here is calculated by [Equation 5](#) using the temperature data over an orbital period:

$$\text{FOM} = \frac{T_{set} \times \int_{\text{period}} dt}{\int_{\text{period}} |T(\theta) - T_{set}| dt}. \quad (\text{Equation 5})$$

However, as plotted in [Figure 3E](#), it is revealed that an optimized TASC ($\epsilon = 0.6$) and an optimized TARC ($\alpha = 0.4$) could have comparable FOMs. The additional advantage of TASCs in this case comes from two aspects: (1) Earth albedo increases the amount of heat flux regulated by TASCs, and (2) Earth thermal IR radiation decreases the cooling efficiency of TARCs.

The above analyses are based on the absence of solar eclipse. Here, we also simulated the scenario where the 1U-CubeSat operates in the geosynchronous orbit in the ecliptic plane ([Figure 3F](#)), namely, the plane that the satellite will experience a solar eclipse during each circulation around the Earth. The transient temperatures of the orbiting CubeSats covered by different TASCs or TARC ([Figures 3G](#) and [3H](#)) show that TARC outperform TASCs in reducing temperature swing of space-crafts in missions. Strikingly, the temperature swing of the CubeSat covered by the low- α (0.1) TARC is merely 0.7°C, even with the solar eclipse at ~12 and ~36 h. Similarly, an optimized α is necessary for the best performance of TARCs, and SP-compatible TARCs can still effectively stabilize the CubeSat temperature. The advantage of TARC over TASC in the presence of eclipse is verified by [Figure 3J](#), where the FOM of an optimized TASC is 189, far lower than that of an optimized TARC (628). More results can be found in [Note S6](#) and [Figures S6](#) and [S7](#).

In-depth comparison of TASCs and TARC in Earth orbits

The transient temperature simulation with and without solar eclipses leads to the comparison between TASCs and TARC in Earth orbits: (1) for space missions without solar eclipses, optimized TASCs and TARC have similar performance in reducing temperature swings; (2) when the space objects are subject to eclipses, TARC are favorable due to their capacity of temperature regulation in the absence of solar light; (3) when used on SPs, TARC performs better than TASCs; and (4) in-depth comparison between TASCs and TARC involves detailed information about the space missions, including the planet thermal IR radiation flux, solar light flux, etc.

This is especially important for deep-space missions. For example, space objects in near-Venus orbits may receive much more solar irradiance and thermal IR radiation from Venus, which adds to the advantage of TASCs. As for near-Earth space objects, however, TARCs are more versatile. Moreover, the SP compatibility is technically more feasible with TARCs. As such, in the next part, we conduct an extensive investigation of transient temperatures of space objects covered by TARCs.

The previous model in [Figure 3](#) only simulates the homogeneous temperature of a CubeSat by assuming that the entire CubeSat reaches thermal equilibrium instantaneously, with no consideration of the internal thermal resistance and resultant temperature inhomogeneity. To account for the temperature evolution of interior components and surfaces, we use a thermal model of CubeSat decomposed into seven nodes. As shown in [Figure 4A](#), nodes #1–#6 are the six surfaces, while node #7 represents all the core components (electronics, battery, etc.) inside the satellite (details in [Note S7](#) and [Figure S8](#)). The heat transfer among the seven nodes is calculated by

$$Q_i(t) = \begin{cases} \frac{T_7(t) - T_i(t)}{R_i}, & i < 7 \\ \sum_{j=1}^6 \frac{T_j(t) - T_7(t)}{R_j}, & i = 7 \end{cases}, \quad (\text{Equation 6})$$

where Q , T , t , and R are the heat transfer power, temperature, time, and thermal resistance, respectively. The initial conditions are the same as those for [Figure 3](#).

As shown in [Figures 4B](#) and [4C](#), the interior components of the CubeSat are effectively protected from temperature swings by a real-TARC: the temperature swing is only 2.6°C in an orbital period of the CubeSat. As a comparison, when the two non-switching references are used (see [Table S3](#) for details), the temperature of node #7 goes extreme, fluctuating by 15.9°C or more around a baseline temperature as high as 79°C or as low as -30°C . The FOM for the real-TARC is 107.3–136.2 times higher than those of the references, and the influence of solar eclipses is negligible with real-TARC. If the CubeSat is completely covered by SPs and SP-compatible coatings, real-TARC can still restrict the temperature swing down to the range of 20.3°C – 25.6°C , far lower than those of interior satellite components in some real space missions ([Table S2](#)). In [Figure 4D](#), we plotted the FOMs and the temperature swings of all six exterior surfaces where SP-compatible coatings are used. With SP-compatible real-TARC equipped, the surface temperatures stay within 19.5°C – 28.7°C , thus efficiently protecting the satellite structures from thermal fatigue damages. Since SPs may benefit from lower temperatures for a higher PV efficiency,⁴³ an ideal thermal design could simultaneously have room temperature interior components and low-temperature exterior SPs, which can be achieved by decreasing the T_{set} of TARC while optimizing the thermal resistances of the satellite ([Note S8](#); [Figures S9](#) and [S10](#)).

TARCs can be realized by phase-change materials (PCMs) such as vanadium dioxide, whose thermal IR properties undergo a reversible, fast, and drastic change upon temperature change crossing its phase-change temperature.^{44–47} The target temperature T_{set} is set by the phase-change temperature of PCMs, which can be engineered by doping,⁴⁸ strain engineering,⁴⁹ etc. Desired ε and α of TASCs and TARCs can be engineered and tuned using artificial photonic structures, respectively.^{22,27,50} Two existing challenges in this field are (1) TARCs were only experimentally demonstrated very recently, and existing designs have not been tested in space conditions,²² and (2) the realization of SP-compatible TASCs and TARCs is an extremely ambitious and challenging task that requires groundbreaking photonic

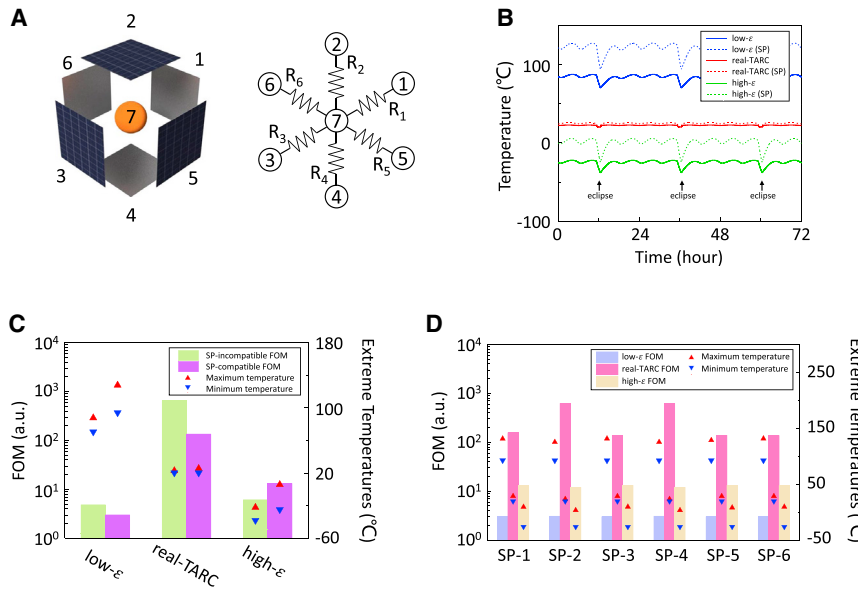


Figure 4. In-depth thermal analysis of solar panels and interior components of a geosynchronous CubeSat covered by TARC in the ecliptic plane

(A) An exploded diagram of the CubeSat (left) and the corresponding thermal resistance circuit (right).

(B) Transient temperatures of node #7.

(C) Extracted FOMs and extreme temperatures of node #7.

(D) Extracted FOMs and extreme temperatures of nodes #1-#6.

design and material engineering. Experimental realization of a functional TASC with a large α tuning range is yet to be demonstrated. Experimental implementation of TASCs and TARCs in space is yet to be achieved.

In conclusion, we systematically and theoretically analyzed the temperature-management performance of TASCs or TARCs for three thermal system models in outer space, eight TASCs or TARCs with different technical parameters, and one case study using data of experimentally realized TARCs. It is found that, though both TASCs and TARCs significantly stabilize the temperature of space objects, TARCs perform significantly better than TASCs due to the broad spectral range for thermal radiation in space, as well as larger physical surface area for thermal emission than for solar absorption. Furthermore, when the temperature-adaptive coatings are designed to be spectrally compatible to SPs, they (especially TARCs) bring great advantages in temperature management without sacrificing the solar power generation of space objects. As a result, thin, light-weight, and cost-effective TARCs show great promise as the future passive TMT for space missions with exceptional temperature-stabilization capabilities.

EXPERIMENTAL PROCEDURES

Resource availability

Lead contact

Further information and requests for resources and materials should be directed to and will be fulfilled by the lead contact, Junqiao Wu (wuj@berkeley.edu).

Materials availability

This study did not generate new unique reagents.

Data and code availability

The data presented in this work are available from the [lead contact](#) upon reasonable request.

SUPPLEMENTAL INFORMATION

Supplemental information can be found online at <https://doi.org/10.1016/j.xcpr.2022.101066>.

ACKNOWLEDGMENTS

This work was supported by US NSF grant no. ECCS-1953803. J.W. acknowledges the Bakar Prize.

AUTHOR CONTRIBUTIONS

K.D. and J.W. conceived the idea. K.D., D.T., J.L., S.W., and J.Y. conducted the modeling and simulation. K.D. wrote the manuscript with assistance from other authors. All authors reviewed and revised the manuscript.

DECLARATION OF INTERESTS

The authors declare no competing interests.

Received: July 25, 2022

Revised: August 22, 2022

Accepted: August 31, 2022

Published: September 20, 2022

REFERENCES

1. J.D. Cressler, and H.A. Mantooth, eds. (2017). Extreme environment electronics (CRC Press). <https://www.routledge.com/Extreme-Environment-Electronics/Cressler-Mantooth/p/book/9781138074224>.
2. Pisacane, V.L. (2003). Spacecraft systems design and engineering. In Encyclopedia of Physical Science and Technology, 3rd ed., R.A. Meyers, ed. (Elsevier Science Ltd), pp. 464–483. <https://doi.org/10.1016/B0-12-227410-5/00888-7>.
3. Karam, R.D. (1998). Satellite thermal control for systems engineers (Vol. 181). In Progress in Astronautics and Aeronautics, P. Zarchan, ed. (Aiaa). <https://doi.org/10.2514/4.866524>.
4. Thirsk, R., Kuipers, A., Mukai, C., and Williams, D. (2009). The space-flight environment: the international space station and beyond. CMAJ (Can. Med. Assoc. J.) 180, 1216–1220. <https://doi.org/10.1503/cmaj.081125>.
5. Toropova, M.M. (2021). Thermally adaptive axissymmetric trusses for satellite platforms. Acta Astronaut. 181, 139–150. <https://doi.org/10.1016/j.actaastro.2021.01.014>.
6. Asmar, S.W., Armstrong, J.W., less, L., and Tortora, P. (2005). Spacecraft Doppler tracking: noise budget and accuracy achievable in precision radio science observations. Radio Sci. 40, 1–9. <https://doi.org/10.1029/2004RS003101>.
7. Delabrouille, J. (1998). Analysis of the accuracy of a destriping method for future cosmic microwave background mapping with the PLANCK SURVEYOR satellite. Astron. Astrophys., Suppl. Ser. 127, 555–567. <https://doi.org/10.1051/aa:1998119>.
8. Pippin, G. (2003). Space environments and induced damage mechanisms in materials. Prog. Org. Coat. 47, 424–431. <https://doi.org/10.1016/j.porgcoat.2003.07.003>.
9. Hengeveld, D., Mathison, M., Braun, J., Groll, E., and Williams, A. (2010). Review of modern spacecraft thermal control technologies. HVAC R Res. 16, 189–220. <https://doi.org/10.1080/10789669.2010.1039090>.
10. (2022). 7.0 Thermal Control (National Aeronautics and Space Administration). <https://www.nasa.gov/smallsat-institute/sst-soa/thermal-control>.
11. He, Y., Li, B., Wang, Z., and Zhang, Y. (2021). Thermal design and verification of spherical scientific satellite Q-SAT. International Journal of Aerospace Engineering, 1–11. <https://doi.org/10.1155/2021/9961432>.
12. Bhatt, J.H., and Barve, J.J. (2019). Control of spaceborne linear cryocoolers: a review. Prog. Aero. Sci. 109, 100544. <https://doi.org/10.1016/j.paerosci.2019.05.004>.
13. Guo, D., Sheng, Q., Dou, X., Wang, Z., Xie, L., and Yang, B. (2020). Application of thermoelectric cooler in temperature control system of space science experiment. Appl. Therm. Eng. 168, 114888. <https://doi.org/10.1016/j.applthermaleng.2019.114888>.
14. Sunada, E., Bhandari, P., Carroll, B., Hendricks, T., Furst, B., Kempenaar, J., et al. (2016). A two-phase mechanically pumped fluid loop for thermal control of deep space science missions. In 46th International Conference on Environmental Systems. <https://tuu-ir.tdl.org/handle/2346/67545>.
15. Liu, T., Sun, Q., Meng, J., Pan, Z., and Tang, Y. (2016). Degradation modeling of satellite thermal control coatings in a low earth orbit environment. Sol. Energy 139, 467–474. <https://doi.org/10.1016/j.solener.2016.10.031>.
16. Baturkin, V. (2005). Micro-satellites thermal control—concepts and components. Acta Astronaut. 56, 161–170. <https://doi.org/10.1016/j.actaastro.2004.09.003>.
17. Kim, Y.S., Lee, E.S., and Woo, S.H. (2003). System trade-off study and opto-thermo-mechanical analysis of a sunshield on the MSC of the KOMPSAT-2. Journal of Astronomy and Space Sciences 20, 393–402. <https://doi.org/10.5140/JASS.2003.20.4.393>.
18. Evans, A.L. (2019, August). Design and testing of the CubeSat form factor thermal control louvers. In 33rd Annual AIAA/USU Conference on Small Satellites. <https://ntrs.nasa.gov/citations/20190028943>.
19. Bacciotti, A., Bucchi, F., Frendo, F., Mameli, M., Perna, R., and Filippeschi, S. (2021, February). On the use of shape memory alloys for deployable passive heat radiators in space satellites. IOP Conf. Ser. Mater. Sci. Eng. 1038, 012061. <https://doi.org/10.1088/1757-899X/1038/1/012061>.

20. Heo, H., Li, S., Bao, H., and Ju, J. (2019). A passive thermal switch with kirigami-inspired mesostructures. *Adv. Eng. Mater.* 21, 1900225. <https://doi.org/10.1002/adem.201900225>.
21. Farid, M.M., Khudhair, A.M., Razack, S.A.K., and Al-Hallaj, S. (2004). A review on phase change energy storage: materials and applications. *Energy Convers. Manag.* 45, 1597–1615. <https://doi.org/10.1016/j.enconman.2003.09.015>.
22. Tang, K., Dong, K., Li, J., Gordon, M.P., Reichertz, F.G., Kim, H., Rho, Y., Wang, Q., Lin, C.Y., Grigoropoulos, C.P., et al. (2021). Temperature-adaptive radiative coating for all-season household thermal regulation. *Science* 374, 1504–1509. <https://doi.org/10.1126/science.abf7136>.
23. Ono, M., Chen, K., Li, W., and Fan, S. (2018). Self-adaptive radiative cooling based on phase change materials. *Opt Express* 26, A777–A787. <https://doi.org/10.1364/OE.26.00A777>.
24. Hippalgaonkar, K. (2022). All-weather thermal regulation coatings. *Joule* 6, 286–288. <https://doi.org/10.1016/j.joule.2022.01.012>.
25. Kim, H., Cheung, K., Auyeung, R.C.Y., Wilson, D.E., Charipar, K.M., Piqué, A., and Charipar, N.A. (2019). VO₂-based switchable radiator for spacecraft thermal control. *Sci. Rep.* 9, 11329–11338. <https://doi.org/10.1038/s41598-019-47572-z>.
26. Sun, K., Xiao, W., Wheeler, C., Simeoni, M., Urbani, A., Gaspari, M., et al. (2022). VO₂ metasurface smart thermal emitter with high visual transparency for passive radiative cooling regulation in space and terrestrial applications. *Nanophotonics*. <https://doi.org/10.1515/nanoph-2022-0020>.
27. Sun, K., Riedel, C.A., Urbani, A., Simeoni, M., Mengali, S., Zalkovskij, M., Bilenberg, B., de Groot, C., and Muskens, O.L. (2018). VO₂ thermochromic metamaterial-based smart optical solar reflector. *ACS Photonics* 5, 2280–2286. <https://doi.org/10.1021/acspophotonics.8b00119>.
28. Xu, X., Gu, J., Zhao, H., Zhang, X., Dou, S., Li, Y., Zhao, J., Zhan, Y., and Li, X. (2022). Passive and dynamic phase-change-based radiative cooling in outdoor weather. *ACS Appl. Mater. Interfaces* 14, 14313–14320. <https://doi.org/10.1021/acsami.1c23401>.
29. Villela, T., Costa, C.A., Brandão, A.M., Bueno, F.T., and Leonardi, R. (2019). Towards the thousandth CubeSat: a statistical overview. *International Journal of Aerospace Engineering*, 1–13. <https://doi.org/10.1155/2019/5063145>.
30. Amores, A.P., Ravishankar, A.P., and Anand, S. (2022, April). Design and modelling of metal-oxide nanodisk arrays for structural colors and UV-blocking functions in solar cell glass covers. *Photonics* 9, 273. <https://doi.org/10.3390/photonics9050273>.
31. Vitanov, P., Delibasheva, M., Goranova, E., and Peneva, M. (2000). The influence of porous silicon coating on silicon solar cells with different emitter thicknesses. *Sol. Energy Mater. Sol. Cells* 61, 213–221. [https://doi.org/10.1016/S0927-0248\(99\)00110-5](https://doi.org/10.1016/S0927-0248(99)00110-5).
32. Yao, Y., Wang, L., Zhu, X., Tu, W., Zhou, Y., Liu, R., Sun, J., Tao, B., Wang, C., Yu, X., et al. (2022). Extraterrestrial photosynthesis by Chang'E-5 lunar soil. *Joule* 6, 1008–1014. <https://doi.org/10.1016/j.joule.2022.04.011>.
33. The national renewable energy laboratory (2022). Solar Spectra. <https://www.nrel.gov/grid/solar-resource/spectra.html>.
34. Chen, Z., Zhu, L., Li, W., and Fan, S. (2019). Simultaneously and synergistically harvest energy from the sun and outer space. *Joule* 3, 101–110. <https://doi.org/10.1016/j.joule.2018.10.009>.
35. Chin, A., Coelho, R., Nugent, R., Munakata, R., and Puig-Suari, J. (2008, September). CubeSat: the pico-satellite standard for research and education. In *AIAA Space 2008 Conference & Exposition*, p. 7734. <https://doi.org/10.2514/6.2008-7734>.
36. Lincot, D. (2017). The new paradigm of photovoltaics: from powering satellites to powering humanity. *C. R. Phys.* 18, 381–390. <https://doi.org/10.1016/j.crhy.2017.09.003>.
37. Zampiva, R.Y., Kaufmann, C.G., Jr., Acauan, L.H., Seeger, R.L., Bonatto, F., Boeira, C.D., Santos, W.Q., Jacinto, C., Figueiroa, C.A., Dornelles, L.S., et al. (2018). Luminescent anti-reflection coatings based on Er³⁺ doped forsterite for commercial silicon solar cells applications. *Sol. Energy* 170, 752–761. <https://doi.org/10.1016/j.solener.2018.05.097>.
38. Garzón, A., and Villanueva, Y.A. (2018). Thermal analysis of satellite libertad 2: a guide to cubesat temperature prediction. *J. Aerosp. Technol. Manag.* 10, E4918. <https://doi.org/10.5028/jatm.v10.1011>.
39. Morsch Filho, E., Nicolau, V.d.P., Paiva, K.V.d., and Possamai, T.S. (2020). A comprehensive attitude formulation with spin for numerical model of irradiance for CubeSats and Picosats. *Appl. Therm. Eng.* 168, 114859. <https://doi.org/10.1016/j.applthermaleng.2019.114859>.
40. Vega Martinez, S., Filho, E.M., Seman, L.O., Bezerra, E.A., Nicolau, V.D.P., Ovejero, R.G., and Leithardt, V.R.Q. (2021). An integrated thermal-electrical model for simulations of battery behavior in CubeSats. *Appl. Sci.* 11, 1554. <https://doi.org/10.3390/app11041554>.
41. Hernández-Gómez, J.J., Yáñez-Casas, G.A., Torres-Lara, A.M., Couder-Castañeda, C., Orozco-del-Castillo, M.G., Valdiviezo-Navarro, J.C., Medina, I., Solís-Santomé, A., Vázquez-Alvarez, D., and Chávez-López, P.I. (2019, November). Conceptual low-cost on-board high performance computing in CubeSat nanosatellites for pattern recognition in Earth's remote sensing. *Proceedings of the 1st International Conference on Geospatial Information Sciences* 13, 114–122. <https://doi.org/10.29007/8d25>.
42. CanX-7 (Canadian Advanced Nanospace eXperiment-7) (2022). ESA Earth Observation Portal. <https://directory.eoportal.org/web/eoportal/satellite-missions/c-missions/canx-7>.
43. Fesharaki, V.J., Dehghani, M., Fesharaki, J.J., and Tavasoli, H. (2011). The effect of temperature on photovoltaic cell efficiency. In *Proceedings of the 1st International Conference on Emerging Trends in Energy Conservation-ETEC*, Tehran, Iran, pp. 20–21. https://research.iaun.ac.ir/pd/jjfesharaki/pdf/PaperC_4124.pdf.
44. Dong, K., Hong, S., Deng, Y., Ma, H., Li, J., Wang, X., Yeo, J., Wang, L., Lou, S., Tom, K.B., et al. (2018). A lithography-free and field-programmable photonic metacanvas. *Adv. Mater.* 30, 1703878. <https://doi.org/10.1002/adma.201703878>.
45. Kats, M.A., Sharma, D., Lin, J., Genevet, P., Blanchard, R., Yang, Z., Qazilbash, M.M., Basov, D.N., Ramanathan, S., and Capasso, F. (2012). Ultra-thin perfect absorber employing a tunable phase change material. *Appl. Phys. Lett.* 101, 221101. <https://doi.org/10.1063/1.4767646>.
46. Wang, S., Jiang, T., Meng, Y., Yang, R., Tan, G., and Long, Y. (2021). Scalable thermochromic smart windows with passive radiative cooling regulation. *Science* 374, 1501–1504. <https://doi.org/10.1126/science.abg0291>.
47. Ke, Y., Yin, Y., Zhang, Q., Tan, Y., Hu, P., Wang, S., Tang, Y., Zhou, Y., Wen, X., Wu, S., et al. (2019). Adaptive thermochromic windows from active plasmonic elastomers. *Joule* 3, 858–871. <https://doi.org/10.1016/j.joule.2018.12.024>.
48. Tang, K., Dong, K., Nicolai, C.J., Li, Y., Li, J., Lou, S., Qiu, C.W., Raulet, D.H., Yao, J., and Wu, J. (2020). Millikelvin-resolved ambient thermography. *Sci. Adv.* 6, eabd8688. <https://doi.org/10.1126/sciadv.abd8688>.
49. Howard, S.A., Evlyukhin, E., Páez Fajardo, G., Paik, H., Schlot, D.G., and Piper, L.F.J. (2021). Digital tuning of the transition temperature of epitaxial VO₂ thin films on MgF₂ substrates by strain engineering. *Adv. Mater. Interfaces* 8, 2001790. <https://doi.org/10.1002/admi.202001790>.
50. Long, L., Taylor, S., and Wang, L. (2020). Enhanced infrared emission by thermally switching the excitation of magnetic polariton with scalable microstructured VO₂ metasurfaces. *ACS Photonics* 7, 2219–2227. <https://doi.org/10.1021/acspophotonics.0c00760>.